AIAA JOURNAL
Vol. 48, No. 7, July 2010

Using Reynolds-Averaged Navier–Stokes Calculations to Predict Trailing-Edge Noise

Stewart Glegg*
Florida Atlantic University, Boca Raton, Florida 33431
Bruce Morin† and Oliver Atassi‡
Pratt and Whitney Aircraft, United Technologies Corporation, East Hartford, Connecticut 06108
and
Ramons Reba‡
United Technologies Research Center, East Hartford, Connecticut 06108

DOI: 10.2514/1.38836

This paper describes a method for using Reynolds-averaged Navier–Stokes calculations of the flow over an airfoil to calculate far-field sound spectra generated by boundary-layer turbulence interacting with the airfoil trailing edge. It is shown that a model of the spatial distribution of turbulent kinetic energy in a boundary-layer flow can be related to an integral of the local turbulence spectrum multiplied by a function of the mean flow velocity distribution. Inverting this relationship gives the turbulence spectrum required for calculations of the pressure on the surface beneath the boundary layer, hence the far-field sound radiated from a turbulent boundary layer interacting with a sharp trailing edge. Results are presented showing estimates of surface pressure spectra and radiated sound from a turbulent boundary layer flowing over the sharp trailing edge of a NACA 0012 airfoil, and they are compared with measurements of airfoils with different chord and Reynolds numbers. Also shown are predictions based on this approach for the self-noise from a 22 in. fan. The measured and predicted far-field sound spectra were found to show the same dependence on flow speed and close agreement in absolute level.

Nomenclature

$a_s(y, k_1, k_3)$	=	vortex sheet strength
b	=	blade semispan
c_o	=	speed of sound
$E()$	=	turbulence energy spectrum
$Ex()$	=	expected value
k_i	=	wave numbers
$L(y)$	=	local turbulence length scale
P_e	=	see Eq. (33)
p	=	pressure
p_s	=	surface pressure
Q_sQ_w	=	see Eq. (38)
q, q_s, q_w	=	turbulent kinetic energy of different components
R	=	nondimensional boundary-layer thickness
Re	=	Reynolds number, $U_\infty\delta_o/\nu$
R_{pp}	=	surface pressure correlation function
S_{aa}	=	wave-number spectrum of the vortex sheet strength
$S_{PP}(k_1, k_3, \omega)$	=	wave-number spectrum of surface pressure
$S_{PP}(\omega)$	=	frequency spectrum of surface pressure
S_{pp}	=	far-field noise spectrum
s_i	=	velocity component defined in Eq. (9)
$\bar{s}_i$	=	nondimensional velocity component defined in Eq. (17)
U_o	=	convection velocity, $-\omega/k_1$, $U(y_o)$
$U(x_2)$	=	mean flow
U_∞	=	freestream velocity outside the boundary layer
U', U'', $\cdots$	=	derivatives with respect to x_2
u	=	v_2
v_i	=	velocity
$\hat{v}_i$, $\hat{\omega}_i$, $\cdots$	=	Fourier transforms defined by Eq. (5)
$\dot{v}_i$, $\dot{\omega}_i$, $\cdots$	=	derivative with respect to time
w_i	=	velocity component defined in Eq. (9)
$\bar{w}_i$	=	nondimensional velocity component defined in Eq. (19)
x_i	=	coordinate system (x_1, x_2, x_3)
y	=	distance from wall, x_2
y_0	=	distance from the wall, where ω is equal to $k_1U(y)$
Γ	=	see Eq. (19)
δ_o	=	boundary-layer thickness
ε	=	dissipation
ε_{ijk}	=	permutation tensor
Λ	=	convective eigenvalue, $-i(\omega + Uk_1)$
Λ_{aa}	=	wave-number spectrum of a
λ	=	$(k_1^2 + k_3^2)^{1/2}$
λ_o	=	$(\omega^2/U_o^2 + k_3^2)^{1/2}$
ν	=	kinematic viscosity
ρ_o	=	mean density
$\psi_j(x_i)$, $\bar{\psi}_j(y_o, k_1, k_3)$	=	vector potentials
Ω	=	mean vorticity, $-\mathrm{d}U/\mathrm{d}x_2$
ω	=	frequency
ω_i	=	vorticity
$\omega_i^{(s)}$	=	vorticity of the s component

I. Introduction

RECENT advances in numerical techniques have resulted in efficient methods for calculating the Reynolds-averaged statistics of the flow around most bodies. These calculations provide the mean flow as well as the local turbulent kinetic energy (TKE) and dissipation. However, they provide no information on the higher order statistics or spectral content of the unsteady part of the flow. For many applications, especially those involving sound radiation, a

Presented as Paper 2993 at the AIAA/CEAS Aeroacoustics Conference, Vancouver, 4–7 May 2008; received 30 May 2008; revision received 25 March 2009; accepted for publication 31 March 2009.

*Professor, Center for Acoustics and Vibration. Associate Fellow AIAA.
†Technical Fellow. Senior Member AIAA.
‡Principal Engineer. Senior Member AIAA.

procedure for estimating the two-point correlation function of the velocity fluctuations throughout the flow is needed. In this paper, we will show how a model of the spatial distribution of TKE in a boundary-layer flow can be related to an integral of the local turbulence spectrum multiplied by a function of the mean flow velocity distribution. Inverting this relationship gives the turbulence spectrum required for calculations of the pressure on the surface beneath the boundary layer, hence the far-field sound radiated from a turbulent boundary layer interacting with a sharp trailing edge (Amiet [1] and Howe [2]).

The concept of using an analytical model of turbulent velocity fluctuations to obtain a description of the two-point statistics in a flow is not new. For example, Townsend [3] studied different types of eddy functions to estimate the two-point correlation tensor of fluctuating velocities in a shear flow. This approach, while giving plausible results, is not based on solutions to the Navier–Stokes equations, and it is rooted in the concept that a turbulent flow can be considered as the linear super position of coherent eddies. More recently, Lee et al. [4] presented calculations of single-point turbulent pressure spectra beneath a boundary layer on a flat plate and in the wake of a backward-facing step. In this study, Reynolds-averaged Navier–Stokes (RANS) calculations of the flow were combined with semiempirical models of the pressure spectrum, which depended on the local TKE, the mean flow velocity profile, and the local turbulence dissipation scale. The calculations showed good agreement with measurements when the turbulence model was anisotropic. A key component of their analysis was the relationship between the TKE and the vertical component of the turbulent velocity fluctuations. This was based on an anisotropy factor, which was estimated from the average of two sets of experimental data from very different flows (one from a rough wall and one from a smooth wall). A similar approach was used by Lutz et al. [5] to calculate trailing-edge noise from wind turbine blades, but the estimates for the radiated noise showed significant error. While these results are very encouraging, they are not based on solutions to the unsteady continuity and momentum equations with the appropriate boundary conditions, which is clearly a limitation for applications involving more general types of flow.

Recently, Spitz [6] used the data from direct numerical simulations of a channel flow carried out by Moser et al. [7] to evaluate the two-point correlation function of the vorticity in the flow next to the wall. The results showed that the vorticity correlation length scale in the direction normal to the wall is only a few percent of the boundary-layer thickness. This leads to the hypothesis that velocity fluctuations in a turbulent shear flow can be modeled by uncorrelated sheets of vorticity. However, a detailed analysis based on the linearized form of the vorticity equation applied to a one-dimensional shear flow has shown this simple model is not complete. A solution, which is consistent with the equations of motion can be specified using a model in which the velocity fluctuations in a two-dimensional (2-D) shear flow are linked to the strength of uncorrelated vortex sheets by a convolution integral. The space–time correlation function of the velocity fluctuations can then be defined in terms of the mean square vortex sheet strength as a function of location in the flow. From this, it is relatively straight forward to also calculate surface pressure spectra and surface pressure wave-number spectra, which are required for aeroacoustic and hydroacoustic calculations.

To apply the preceding approach to a particular flow the mean square vortex sheet strength needs to be determined, and we will show how this can be obtained from RANS calculations of the distribution of TKE. The analytical model can be extended to give the space–time correlation function of the velocity fluctuations in the flow. The resulting relationship specifies the TKE as a function of the mean flow profile, a length scale based on dissipation, and the mean square vortex sheet strength. A RANS calculation of the flow provides the mean flow, the length scale, and the TKE; hence, the only unknown is the vortex sheet strength. A complete solution is then obtained by numerically inverting the relationship between the TKE and the vortex sheet strength.

In the following sections an analytical model of an unsteady 2-D shear flow is developed using the linearized equations of motion for small perturbations about the mean flow, with the effect of viscosity suppressed. A four-dimensional solution to the vorticity equation is obtained in terms of a function, which is a solution to Rayleigh's equation. It is then shown that the velocity mode in a boundary layer (or any other 2-D shear flow) consists of two orthogonal components: the s component, which has no vorticity in the direction normal to the surface, and the w component, which has no velocity perturbation in the direction normal to the surface. The solution to Poisson's equation for the pressure shows that the w mode does not cause any pressure fluctuations, and it is also shown that the w gust is convected with the local mean flow. The s component is entirely responsible for pressure perturbations in the flow, and the vorticity of the s component is convected with the local mean flow. The s component can be modeled by the superposition of uncorrelated vortex sheets, which are particularly simple to evaluate analytically.

The method described previously has been used to calculate the surface pressure spectra and radiated sound from a turbulent boundary layer flowing over the sharp trailing edge of a NACA 0012 airfoil, and the results have been compared with the measurements of Brooks and Hodgson [8] and Brooks et al. [9]. The calculations were carried out using RANS estimates of the turbulent boundary-layer flow at 99% of the blade chord. Also given are predictions based on this approach for the self-noise from a 22 in. fan. In addition, we have applied this model to measurements of wind-tunnel boundary-layer velocity fluctuations (Klebanoff [10]) and inverted the measured TKE to obtain one of the three components of the unsteady velocity with some success.

II. Vorticity Formulation for a Parallel Boundary Layer

A. Modeling the Flow

The objective of this section is to derive an analytical model for the unsteady flow in a boundary layer. We will assume that the flow is incompressible and statistically stationary in time and statistically homogeneous in two of its three space dimensions. This assumption implies that the boundary layer is evolving slowly and is not influenced by rapid spatial changes near transition or separation points. Also, we will develop a linear model for the flow disturbances and it should be noted that this approach cannot explicitly capture the streamwise streaky behavior observed in turbulent boundary layers.

We define a coordinate system (x_1, x_2, x_3) in which x_1 is in the direction of the flow and the boundary lies in the plane $x_2 = 0$. All lengths are normalized by the boundary-layer thicknessδ_o and velocities by the freestream velocity outside the boundary layer U_∞. The flow in the boundary layer is governed by the vorticity and continuity equations:

$$\frac{\partial \omega_i}{\partial t} + v_j \frac{\partial \omega_i}{\partial x_j} - \omega_j \frac{\partial v_i}{\partial x_j} - \frac{1}{Re} \frac{\partial^2 \omega_i}{\partial x_j^2} = 0 \tag{1}$$

$$\frac{\partial v_i}{\partial x_i} = 0 \tag{2}$$

$$\omega_i = \varepsilon_{ijk} \frac{\partial v_j}{\partial x_k} \tag{3}$$

where $Re = U_\infty \delta_o / \nu$ is the Reynolds number, ν is the kinematic viscosity, and ε_{ijk} is the permutation tensor. In these equations, v_i is the velocity and ω_i is the vorticity vector.

We assume that the unsteady flow is governed by small fluctuations about a parallel mean flow and that the effects of viscosity do not modify the unsteady fluctuations. The mean flow is given by $U(x_2)$, and the mean vorticity is $\Omega = -\mathrm{d}U/\mathrm{d}x_2$. If we take the time derivative of the vorticity equation (1) and linearize about the mean flow, neglecting the viscous term, we obtain

$$\frac{\mathrm{D}_0 \dot{\omega}_1}{\mathrm{D}t} - \Omega \frac{\partial \dot{v}_3}{\partial x_1} = 0 \tag{4a}$$

$$\frac{\mathrm{D}_0\dot{\omega}_2}{\mathrm{D}t} - \Omega\frac{\partial\dot{v}_2}{\partial x_3} = 0 \tag{4b}$$

$$\frac{\mathrm{D}_0\dot{\omega}_3}{\mathrm{D}t} + \dot{v}_2\frac{\partial\Omega}{\partial x_2} - \Omega\frac{\partial\dot{v}_3}{\partial x_3} = 0 \tag{4c}$$

where $\frac{\mathrm{D}_0}{\mathrm{D}t} \equiv \frac{\partial}{\partial t} + U\frac{\partial}{\partial x_1}$, and Eq. (4a) was simplified by noting that $\omega_2 - \partial v_1/\partial x_3 = -\partial v_3/\partial x_1$.

We will analyze the flow by using the Fourier transforms of the unsteady velocity and vorticity with respect to time, x_1 and x_3, defined as

$$\begin{aligned}
&-i\omega\hat{v}_i(\omega, k_1, k_3, x_2)\\
&\quad= \frac{1}{(2\pi)^3}\int_{-T}^{T}\int_{-R_o}^{R_o}\int_{-R_o}^{R_o}\dot{v}_i(t, x_i)e^{i\omega t + ik_1x_1 + ik_3x_3}\,\mathrm{d}t\,\mathrm{d}x_1\,\mathrm{d}x_3;\\
&-i\omega\hat{\omega}_i(\omega, k_1, k_3, x_2)\\
&\quad= \frac{1}{(2\pi)^3}\int_{-T}^{T}\int_{-R_o}^{R_o}\int_{-R_o}^{R_o}\dot{\omega}_i(t, x_i)e^{i\omega t + ik_1x_1 + ik_3x_3}\,\mathrm{d}t\,\mathrm{d}x_1\,\mathrm{d}x_3
\end{aligned} \tag{5}$$

where ω without a subscript is the angular frequency, k_1 and k_3 are the wave numbers in the x_1 and x_3 directions, and T and R_o tend to infinity. As a consequence, the vorticity and continuity equations in transformed space take the form:

$$\Lambda\hat{\omega}_1 = ik_1\frac{\mathrm{d}U}{\mathrm{d}x_2}\hat{v}_3 \tag{6a}$$

$$\Lambda\hat{\omega}_2 = ik_3\frac{\mathrm{d}U}{\mathrm{d}x_2}\hat{v}_2 \tag{6b}$$

$$\Lambda\hat{\omega}_3 = ik_3\frac{\mathrm{d}U}{\mathrm{d}x_2}\hat{v}_3 + \frac{\mathrm{d}^2U}{\mathrm{d}x_2^2}\hat{v}_2 \tag{6c}$$

$$\hat{v}_1 = -\frac{k_3}{k_1}\hat{v}_3 + \frac{1}{ik_1}\frac{\mathrm{d}\hat{v}_2}{\mathrm{d}x_2} \tag{6d}$$

where $\Lambda = -i(\omega + Uk_1)$ is the convective eigenvalue.

It is shown in the Appendix that these equations can be solved to give a solution for the velocity perturbations in terms of a single function $u(\omega, k_1, k_3, x_2)$ as

$$\begin{aligned}
\hat{v}_1 &= -\frac{ik_1}{\lambda^2}\left(u' + \frac{k_3^2U'u}{k_1^2(U-U_o)}\right); \qquad \hat{v}_2 = u;\\
\hat{v}_3 &= -\frac{ik_3}{\lambda^2}\left(u' - \frac{U'u}{(U-U_o)}\right)
\end{aligned} \tag{7}$$

where the primes denote differentiation with respect to the direction normal to the wall, $\lambda^2 = k_1^2 + k_3^2$, and $\frac{\omega}{k_1} = -U_0$. These results show that the shear in the mean flow introduces a source of unsteady perturbation, which is singular at $y = y_0$, where $U(y_0) = U_0$, unless $u \sim \mathcal{O}(U - U_o)$.

It is also shown in the Appendix that the differential equation for u takes the form of Rayleigh's equation:

$$u'' - \left(\lambda^2 + \frac{U''}{(U-U_o)}\right)u = 0 \tag{8}$$

In conclusion, Eq. (7) gives an analytical model for the three-dimensional unsteady velocity components in a boundary-layer flow, which depends on a solution to Rayleigh's equation. The model assumes a linearized homogeneous turbulent flow in two space dimensions and that the flow statistics are stationary in time. Viscous terms have been ignored.

B. *s* and *w* Velocity Components

The velocity perturbation given by Eq. (7) can be split into two parts

$$\begin{aligned}
\hat{v}_i &= \hat{s}_i + \frac{\hat{w}_iU'}{k_1(U-U_0)}; \qquad \hat{s}_i = \left\{\frac{-ik_1u'}{\lambda^2}, u, \frac{-ik_3u'}{\lambda^2}\right\}_i\\
\hat{w}_i &= \left\{\frac{-ik_3^2u}{\lambda^2}, 0, \frac{ik_3k_1u}{\lambda^2}\right\}_i
\end{aligned} \tag{9}$$

which we will refer to as the s and w components. These two components are orthogonal and divergence free. The s component has no vorticity in the x_2 direction and the w component has no velocity in the x_2 direction. Note that a similar family of solutions exists for perturbations to a parallel flow in an annular geometry (Atassi [11]). The vorticity of the s component is defined as

$$\hat{\omega}_j^{(s)} = \left\{\frac{-ik_3u''}{\lambda^2} + ik_3u, 0, \frac{ik_1u''}{\lambda^2} + ik_1u\right\}_j \tag{10}$$

but since u is a solution to Rayleigh's Eq. (8), this reduces to

$$\hat{\omega}_j^{(s)} = \frac{-iU''u}{\lambda^2(U-U_o)}\{k_3, 0, -k_1\}_j \tag{11}$$

Hence, by substituting $U_0 = -\omega/k_1$ and assuming no instability waves or singularities associated with u, the inverse Fourier transform of Eq. (11) gives the vorticity of the s component as

$$\begin{aligned}
\omega_j^{(s)}(x_i, t) &= -i\int_{-\infty}^{\infty}\int_{-\infty}^{\infty}\int_{-\infty}^{\infty}u(\omega, k_1, k_3, x_2)\\
&\quad\times U''(x_2)e^{-i\omega t - ik_1x_1 - ik_3x_3}\{k_3, 0, -k_1\}_j\frac{k_1\mathrm{d}k_1\mathrm{d}k_3\mathrm{d}\omega}{\lambda^2(k_1U+\omega)}\\
&= -2\pi\int_{-\infty}^{\infty}\int_{-\infty}^{\infty}u(-k_1U, k_1, k_3, x_2)\\
&\quad\times U''(x_2)e^{-ik_1(x_1-Ut)-ik_3x_3}\{k_3, 0, -k_1\}_j\frac{k_1\mathrm{d}k_1\mathrm{d}k_3}{\lambda^2}
\end{aligned} \tag{12}$$

Equation (12) shows that the vorticity of the s component is simply convected by the local mean flow. We can rewrite Eq. (12) so that it represents the vorticity as the superposition of a set of vortex sheets with an amplitude $a_s(y_o, k_1, k_3)$. This rearrangement gives

$$\begin{aligned}
\omega_j^{(s)}(x_i, t) &= \int_0^{\infty}\int_{-\infty}^{\infty}\int_{-\infty}^{\infty}a_s(y_o, k_1, k_3)\\
&\quad\times\delta(y_o - x_2)e^{-ik_1(x_1-U_ot)-ik_3x_3}\{k_3, 0, -k_1\}_j\frac{k_1\,\mathrm{d}k_1\,\mathrm{d}k_3\,\mathrm{d}y_o}{\lambda^2}
\end{aligned} \tag{13}$$

with

$$a_s(y_o, k_1, k_3) = -2\pi u(-k_1U_o, k_1, k_3, y_o)U''(y_o)$$

and y_o is defined as the location where $U = U_o$. Note that the vortex sheet strength a_s will be zero when the rate of change of shear in the mean flow U'' is zero, and so the vortex sheet strength is zero outside the boundary layer or at points of inflection within the boundary layer. Equation (13) also shows that the s component of the flow is induced by the superposition of vortex sheets at the height y_o above the surface.

C. Induced Velocity Field

The s component of the turbulent flow is equivalent to the velocity field induced by a superposition of vortex sheets, and so we can define an associated vector potential, which is the solution to the equation $\nabla^2\psi_j = -\omega_j^{(s)}$, that can be solved subject to the nonpenetration boundary condition at the wall by introducing image vorticity below the wall. The integral (13) implies that we can define $\psi_j(x_i)$ as the superposition of the vector potentials $\bar{\psi}_j(x_2, y_o, k_1, k_3)$, so

$$\begin{aligned}
\psi_j &= \int_0^{\infty}\int_{-\infty}^{\infty}\int_{-\infty}^{\infty}a_s(y_o, k_1, k_3)\bar{\psi}_j(x_2, y_o, k_1, k_3)\\
&\quad\times e^{-ik_1(x_1-U_ot)-ik_3x_3}\,\mathrm{d}k_1\,\mathrm{d}k_3\,\mathrm{d}y_o
\end{aligned} \tag{14}$$

and, with image vorticity included to account for the boundary condition, it follows from Eq. (13) that

$$\frac{\partial^2 \bar{\psi}_j}{\partial x_2^2} - \lambda^2 \bar{\psi}_j = -\frac{k_1}{\lambda^2}[\delta(x_2 - y_o) - \delta(x_2 + y_o)]\{k_3, 0, -k_1\}_j \quad (15)$$

The solution to this equation is given by

$$\bar{\psi}_j = \frac{k_1}{2\lambda^3}(e^{-\lambda|x_2 - y_o|} - e^{-\lambda|x_2 + y_o|})\{k_3, 0, -k_1\}_j \quad (16)$$

Taking the curl of this result gives the velocity as

$$\begin{aligned} \bar{s}_1 &= \frac{k_1^2}{2\lambda^2}(\mathrm{sgn}(x_2 - y_o)e^{-\lambda|x_2 - y_o|} - e^{-\lambda|x_2 + y_o|}); \\ \bar{s}_2 &= \frac{ik_1}{2\lambda}(e^{-\lambda|x_2 - y_o|} - e^{-\lambda|x_2 + y_o|}); \qquad \bar{s}_3 = \frac{k_3 \bar{s}_1}{k_1} \end{aligned} \quad (17)$$

which may be combined with Eq. (14) to give the s component of the velocity as

$$\begin{aligned} s_j(\mathbf{x}, t) = &\int_0^\infty \int_{-\infty}^\infty \int_{-\infty}^\infty a_s(y_o, k_1, k_3)\bar{s}_j(x_2, y_o, \lambda) \\ &\times e^{-ik_1(x_1 - U_o t) - ik_3 x_3}\, \mathrm{d}k_1\, \mathrm{d}k_3\, \mathrm{d}y_o \end{aligned} \quad (18)$$

The equivalent result for the w component of the velocity is obtained by taking the inverse Fourier transform of Eq. (9) and rearranging the result, as was done for Eq. (13), as

$$\begin{aligned} w_j(\mathbf{x}, t) = &\int_0^\infty \int_{-\infty}^\infty \int_{-\infty}^\infty a_s(y_o, k_1, k_3)\bar{w}_j(k_1, k_3)\Gamma(y_o)\delta(x_2 - y_o) \\ &e^{-ik_1(x_1 - U_o t) - ik_3 x_3}\, \mathrm{d}k_1\, \mathrm{d}k_3\, \mathrm{d}y_o \\ \bar{w}_j(k_1, k_3) = &\frac{k_3}{\lambda^2}\{k_3, 0, -k_1\}_j \qquad \Gamma(y_o) = \frac{U'(y_o)}{U''(y_o)} \end{aligned} \quad (19)$$

Hence, the w component of the velocity represents a turbulent gust, which is parallel to the wall and convected by the local mean flow. If the mean shear is almost linear (i.e., $U''(y) \ll 1$), then these components dominate the turbulent flow.

We can define the total velocity as the sum of Eqs. (18) and (19):

$$\begin{aligned} v_j(\mathbf{x}, t) = &\int_0^\infty \int_{-\infty}^\infty \int_{-\infty}^\infty a_s(y_0, k_1, k_3)[\bar{s}_j(x_2, y_0, \lambda) \\ &+ \bar{w}_j(k_1, k_3)\Gamma(y_o)\delta(x_2 - y_o)]e^{-ik_1(x_1 - U_o t) - ik_3 x_3}\, \mathrm{d}k_1\, \mathrm{d}k_3\, \mathrm{d}y_o \end{aligned} \quad (20)$$

The unsteady velocity in a turbulent boundary layer is completely described by this equation, the only unknown being the vortex sheet amplitude a_s. The effect of viscosity has been suppressed but it is not entirely clear that viscosity has been ignored. Adding viscosity will affect the form of Eq. (8), which will alter the solution for u. However, this parameter has been absorbed into the unknown function a_s, and so the viscous solution for u is not required. It is also interesting to note that a solution has been obtained for the linearized unsteady velocity in a boundary layer without the need to compute a numerical solution to Rayleigh's equation (or the Orr–Sommerfield equation for viscous flows).

III. Statistics of the Turbulent Flow

In the previous section, an analytical model of the velocity fluctuations in the boundary layer was described. In this section, we will consider the time-averaged statistics of the flow and derive expressions for the TKE and the surface pressure wave-number spectrum.

A. Turbulent Kinetic Energy

It is assumed that the statistics of the flow perturbations are homogeneous in x_1 and x_3 and stationary in time, which implies that the boundary layer is evolving slowly and is not influenced by rapid spatial changes near transition or separation points. It follows that $u(\omega, k_1, k_3, x_2)$ is uncorrelated at different wave numbers and frequencies. Since y_o is a function of ω/k_1 the stochastic variable $a_s(y_o, k_1, k_3)$ will be uncorrelated for different values of y_o, providing the mean flow is monotonically increasing as a function of distance from the surface and the mean flow profile not does contain any inflection points. Consequently, we can define

$$\begin{aligned} &Ex[a_s(y_o, k_1, k_3)a_s(y_o', k_1', k_3')] \\ &\quad = S_{aa}(y_o, k_1, k_3)(\eta \exp(-2\eta|y_o - y_o'|))\delta(k_1 - k_1')\delta(k_3 - k_3') \end{aligned} \quad (21)$$

where S_{aa} is the spectrum of the vortex sheet strength and is normalized so that

$$\begin{aligned} &Ex[a_s(y_o, k_1, k_3)a_s(y_o, k_1', k_3')] \\ &\quad = \eta(k_1, k_3)S_{aa}(y_o, k_1, k_3)\delta(k_1 - k_1')\delta(k_3 - k_3') \end{aligned} \quad (22)$$

where η is a nondimensional scale and $\eta \exp(-2\eta|y|)$ tends to a Dirac delta function when η is large. Equation (21) implies that the vortex sheets are uncorrelated with height above the surface in this limit.

The contribution to the TKE from the s component can be defined using Eq. (18) as

$$\begin{aligned} q_s(x_2) &= \left(\frac{1}{2}\right) Ex[|s_i|^2] \\ &= \int_0^R \int_{-\infty}^\infty \int_{-\infty}^\infty S_{aa}(y_o, k_1, k_3)\hat{q}_s(x_2, y_o, \lambda)\left(\frac{k_1^2}{\lambda^2}\right) \mathrm{d}k_1\, \mathrm{d}k_3\, \mathrm{d}y_o \end{aligned} \quad (23)$$

where

$$\hat{q}_s(x_2, y_o, \lambda) = (e^{-2\lambda|x_2 - y_o|} + e^{-2\lambda|x_2 + y_o|} - 2H(x_2 - y_o)e^{-2\lambda x_2})/4 \quad (24)$$

and $H(x)$ is the Heaviside function. We can also evaluate the contribution to the TKE by the w component, using Eq. (19) as

$$\begin{aligned} q_w(x_2) &= \left(\frac{1}{2}\right) Ex[|w_i|^2] \\ &= \frac{\Gamma(x_2)^2}{2}\int_{-\infty}^\infty \int_{-\infty}^\infty \eta S_{aa}(x_2, k_1, k_3)\left(\frac{k_3^2}{\lambda^2}\right) \mathrm{d}k_1\, \mathrm{d}k_3 \end{aligned} \quad (25)$$

Since the s and the w velocity components are orthogonal, the total TKE is the sum of these two contributions $q = q_s + q_w$.

B. Solving for the Vortex Sheet Strength

Given the model for the TKE, we will now show how a known distribution of TKE can be used to obtain the spectrum of the vortex sheet strength. To achieve this, we must assume a functional form for the wave-number dependence of the spectrum and a local length scale, which applies to the sheet. We will assume that

$$S_{aa}(y_o, k_1, k_3) = A(y_o)E(\lambda L); \qquad \int_0^\infty E(\lambda L)\eta\lambda\, \mathrm{d}\lambda = C/RL^2 \quad (26)$$

where $L(y_o)$ is the local length scale of the turbulence, which is assumed to be the same in both the spanwise and the flow directions, and R is the nondimensional boundary-layer thickness. The function $\lambda E(\lambda L)$ represents the energy spectrum of the turbulence and is assumed here to be isotropic (in contrast to earlier studies by Lee et al. [4], who used an anisotropic turbulence model). The model for the s component of the TKE then becomes

$$q_s(x_2) = \pi \int_0^R \int_0^\infty A(y_o)\hat{q}_s(x_2, y_o, \lambda)E(\lambda L)\lambda\, \mathrm{d}\lambda\, \mathrm{d}y_o \quad (27)$$

Similarly, for the w component of the TKE, we obtain

$$q_w(x_2) = \frac{\pi\Gamma^2(x_2)}{2R}A(x_2)\int_0^\infty E(\lambda L)\eta\lambda\,\mathrm{d}\lambda = \frac{\pi C\Gamma^2(x_2)}{2RL^2}A(x_2) \tag{28}$$

Given these models and an assumed length-scale distribution, we can (in principle) invert a known distribution of TKE to obtain the unknown function $A(y_o)$, providing, of course, that it is unambiguously defined.

C. Other Flow Parameters

Of particular interest in problems associated with hydroacoustics and aeroacoustics is the wave-number spectrum of the surface pressure below the boundary layer. The unsteady surface pressure can be obtained from the linearized form of Poisson's equation (Townsend [3]),

$$\nabla^2 p = -2U'\frac{\partial v_2}{\partial x_1} \tag{29}$$

which depends on the velocity perturbation in the x_2 direction. It follows that the w component has no influence on the pressure in the flow. Using Eq. (18), we can specify

$$\nabla^2 p = \int_0^\infty\int_{-\infty}^\infty\int_{-\infty}^\infty 2ik_1 a_s(y_o,k_1,k_3)\bar{s}_2(x_2,y_o,\lambda) \times U'(x_2)e^{-ik_1(x_1-U_o t)-ik_3x_3}\,\mathrm{d}k_1\,\mathrm{d}k_3\,\mathrm{d}y_o \tag{30}$$

Taking the Fourier transform of this with respect to x_1 and x_3 gives

$$\frac{\partial^2\hat{p}}{\partial x_2^2} - \lambda^2\hat{p} = \int_0^\infty 2ik_1 a_s(y_o,k_1,k_3)\bar{s}_2(x_2,y_o,\lambda)U'(x_2)e^{ik_1U_o t}\,\mathrm{d}y_o \tag{31}$$

The solution to this equation is given by

$$\hat{p} = \frac{1}{\lambda}\int_0^\infty\int_0^\infty ik_1 a_s(y_o,k_1,k_3)\bar{s}_2(y,y_o,\lambda)U'(y)e^{ik_1U_o t}(e^{-\lambda|x_2-y|} + e^{-\lambda|x_2+y|})\,\mathrm{d}y_o\,\mathrm{d}y \tag{32}$$

Hence, on the surface, where $x_2 = 0$, we obtain

$$p_s(x_1,x_3,t) = \int_0^\infty\int_{-\infty}^\infty\int_{-\infty}^\infty a_s(y_o,k_1,k_3)P_e(y_o,\lambda) \times e^{-ik_1(x_1-U_o t)-ik_3x_3}\left(\frac{k_1}{\lambda}\right)^2\mathrm{d}k_1\,\mathrm{d}k_3\,\mathrm{d}y_o;$$

$$P_e(y_o,\lambda) = \int_0^\infty (e^{-\lambda|y-y_o|} - e^{-\lambda|y+y_o|})U'(y)e^{-\lambda|y|}\,\mathrm{d}y \tag{33}$$

The surface pressure correlation function will then be

$$R_{PP}(\mathbf{x},\mathbf{x}',\tau) = \int_0^R\int_{-\infty}^\infty\int_{-\infty}^\infty A(y_o)|P_e|^2\left(\frac{k_1^4}{\lambda^4}\right)E(\lambda L) \times e^{-ik_1(x_1-x_1')-ik_3(x_3-x_3')+ik_1U_o\tau}\,\mathrm{d}k_1\,\mathrm{d}k_3\,\mathrm{d}y_o \tag{34}$$

and it follows that the wave-number spectrum of the surface pressure fluctuations is

$$S_{PP}(k_1,k_3,\omega) = \int_0^R \frac{k_1^4 A(y_o)}{\lambda^4}|P_e(y_o,\lambda)|^2 \times E(\lambda L)\,\delta(k_1U(y_o)+\omega)\,\mathrm{d}y_o \tag{35}$$

In addition, we will also find it useful to evaluate the surface pressure spectrum, given in dimensional terms, by

$$S_{PP}(\omega) = \frac{(\rho_o U_\infty^2)^2\delta_o}{U_\infty}\int_{-\infty}^\infty\int_{-\infty}^\infty S_{PP}(k_1,k_3,\omega)\,\mathrm{d}k_1\,\mathrm{d}k_3 = \frac{(\rho_o U_\infty^2)^2\delta_o}{U_\infty}\int_0^R\int_{-\infty}^\infty \frac{\omega^4 A(y_o)}{U_o^5\lambda_o^4}|P_e(y_o,\lambda_o)|^2E(\lambda_o L)\,\mathrm{d}k_3\,\mathrm{d}y_o \tag{36}$$

where $\lambda_o^2 = \omega^2/U_o^2 + k_3^2$, and we note that all terms inside the integral are nondimensional.

Finally, trailing-edge noise can be estimated at 90 deg to the span and at an angle θ to the flow direction for an observer at $\mathbf{x}$ using (Howe [2], equation 3.5.14)

$$S_{pp}(\mathbf{x},\omega) = \frac{\omega b\sin^2(\theta/2)(\rho_o U_\infty^2)\delta_o^2}{2\pi c_o|\mathbf{x}|^2}\int_{-\infty}^\infty \frac{S_{PP}(k_1,0,\omega)}{|k_1|}\,\mathrm{d}k_1 = \frac{b\sin^2(\theta/2)(\rho_o U_\infty^2)\delta_o^2}{2\pi c_o|\mathbf{x}|^2}\int_0^R A(y_o)|P_e\left(y_o,\frac{\omega}{U_o}\right)|^2E\left(\frac{\omega L}{U_o}\right)\mathrm{d}y_o \tag{37}$$

where $2b$ is the blade span, $S_{pp}(\mathbf{x},\omega)$ is the two-sided spectrum, and all terms inside the integral are nondimensional.

IV. Inverting the Turbulent Kinetic Energy Distribution

To obtain the vortex sheet strength $A(y_o)$, we combine Eqs. (27) and (28) to obtain the total TKE q as

$$q(x_2) = \int_0^R A(y_o)[Q_s(x_2,y_o) + Q_w(y_o)\delta(x_2-y_o)]\,\mathrm{d}y_o;$$

$$Q_s(x_2,y_o) = \pi\int_0^\infty \hat{q}_s(x_2,y_o,\lambda)E(\lambda L)\lambda\,\mathrm{d}\lambda;$$

$$Q_w(y_o) = \frac{\pi C}{2RL^2(y_o)}\left(\frac{U'(y_o)}{U''(y_o)}\right)^2 \tag{38}$$

The numerical inversion of Eq. (38) is then achieved by defining $q_m = q(m\Delta y)$,

$$Q_{mn} = Q_s(m\Delta y, n\Delta y)\Delta y + Q_w(m\Delta y)\delta_{mn}$$

and $A_n = A(n\Delta y)$, so

$$A_n = [Q_{mn}]^{-1}q_m \tag{39}$$

By combining the integral in Eq. (38) with Eq. (24), we find that

$$Q_s = (\pi/4L^2)\{F(|x_2-y_o|/L) + F[(x_2+y_o)/L] - 2F(x_2/L)H(x_2-y_o)\} \tag{40}$$

where

$$F(x/L) = L^2\int_0^\infty e^{-2\lambda x}E(\lambda L)\lambda\,\mathrm{d}\lambda \tag{41}$$

which is simply the Laplace transform of $\lambda E(\lambda L)$, and so it can be readily obtained for a variety of functions.

Various alternatives have been considered for the energy spectrum $\lambda E(\lambda L)$. Pope [12] suggested that the energy spectrum should be of the form

$$(\lambda L)E(\lambda L) = (\lambda L)^{-5/3}f_L(\lambda L)f_\eta(\lambda\eta) \tag{42}$$

where f_L and f_η are nondimensional functions and $\eta = (\nu^3/\varepsilon)^{1/4}$ is the dissipation length scale. For high-Reynolds-number flows, it can be assumed that $f_\eta = 1$, and Pope [12] gives

$$f_L(\xi) = \left(\frac{\xi}{(c_L+\xi^2)^{1/2}}\right)^{5/3+p} \tag{43}$$

where p is an integer. Modeling of turbulence in aeroacoustic applications is often based on the von Karman spectrum, for which $p = 4$ and $c_L = 1$, but Pope [12] suggests that, for high Reynolds numbers, a better fit to the spectrum of homogeneous turbulence at low frequencies is obtained if $p = 2$ and $c_L = 6.78$. In this study, it was found that the best fit to the data in a high-Reynolds-number boundary-layer flow over an airfoil was given by using

$$f_L(\xi) = \left\{1 + \frac{c_R}{\xi^3}\right\}\left(\frac{\xi}{(1+\xi^2)^{1/2}}\right)^{17/3}; \qquad c_R = 0.05 \qquad (44)$$

This is equivalent to using the von Karman spectrum at high frequencies, but is modified so that the low frequency asymptote of the spectrum is $\sim\xi$. The three alternative spectra are shown in Fig. 1. In addition, we will model the constant C as

$$C = \int_0^\omega (\eta R) E(\xi)\xi d\xi \approx k \int_0^\omega E(\xi)\xi d\xi$$

where $k = 0.5$ was used throughout this study.

The choice for the length scale is an important factor, which impacts the turbulence model. Townsend [3] reviewed wind-tunnel data of turbulent boundary layers and concluded that $L = y_o$ was the best fit to the majority of the data. This implies that the vortex scale increases linearly with distance from the wall. However, this assumption gives very large scales in the outer part of the boundary layer, and a dissipation scale would appear to be more appropriate in that region. It was found that, for a turbulent boundary layer over a NACA 0012 airfoil (as described below), the length scale $q^{3/2}/\varepsilon$ (where q is the TKE and ε is the dissipation) was $\sim 2y_o$ in the near-wall region and asymptotes to a constant value in the outer part of the boundary layer. Consequently, we have chosen

$$L = q^{3/2}/2\varepsilon \qquad (45)$$

We have also considered the wind-tunnel measurements of a turbulent boundary layer by Klebanoff [10], for which the dissipation as a function of height above the wall was not available. In this case, the mixing length scale was used and adjusted so that its slope at the wall gave $L \sim y_o$. In this case,

$$L = \frac{\sqrt{\langle v_1 v_2\rangle}}{0.4|U'|} \qquad (46)$$

Figure 2 shows how these two alternative definitions compare with Townsend's [3] model. Remarkably, for the two cases considered (one of which is based on RANS calculations on an airfoil and the other on wind-tunnel data) give very similar length-scale distributions across the boundary layer.

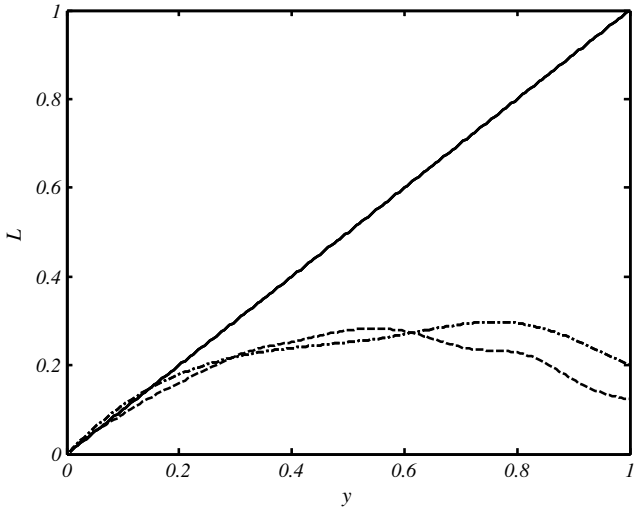

Fig. 2 The length-scale models obtained using either Eq. (45) (dashed-dotted line) or Eq. (46) (dashed line), based on different data sets, compared with Townsend's model (solid line) [3].

V. Wind-Tunnel Boundary-Layer Measurements

This section describes how measured values of TKE in the boundary layer of a wind-tunnel wall can be used to estimate the unsteady turbulent stresses. Klebanoff [10] gives wind-tunnel measurements of the turbulent stresses in a boundary layer with a Reynolds number based on momentum thickness of 6955. The TKE can be obtained from the three components of the velocity and then inverted to obtain the distribution function $A(y_o)$. The accuracy of the modeling can then be evaluated by calculating the upwash component of the velocity based on the theory described previously by using

$$\langle v_2(x_2)^2\rangle = \int_0^R A(y_o)\left\{\frac{\pi}{4}\int_0^\infty (e^{-\lambda|x_2-y_o|} - e^{-\lambda(x_2+y_o)})^2 E(\lambda L)\lambda\, d\lambda\right\} dy_o \qquad (47)$$

To carry out the calculations we have assumed a power-law relationship for the mean velocity profile with $U \sim x_2^{1/7}$ and the length-scale distribution specified by Eq. (46). The inversion of the TKE was carried out using 200 points equally spaced between the wall and $x_2 = 1.1$.

Figure 3 shows the TKE and the measured and estimated values of the mean square velocity normal to the wall. The accuracy of the estimate is not particularly good. However, the instrumentation used for the measurement of the turbulent velocities may have been limited by its frequency response and so the model used here may be

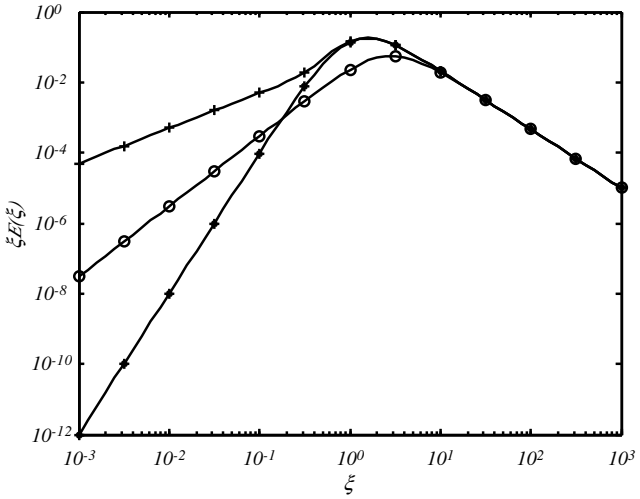

Fig. 1 Energy spectra considered to model the flow in a turbulent boundary layer in a high-Reynolds-number flow (von Karman spectrum: asterisks, Pope spectrum [12]: circles, modified von Karman spectrum: plus signs).

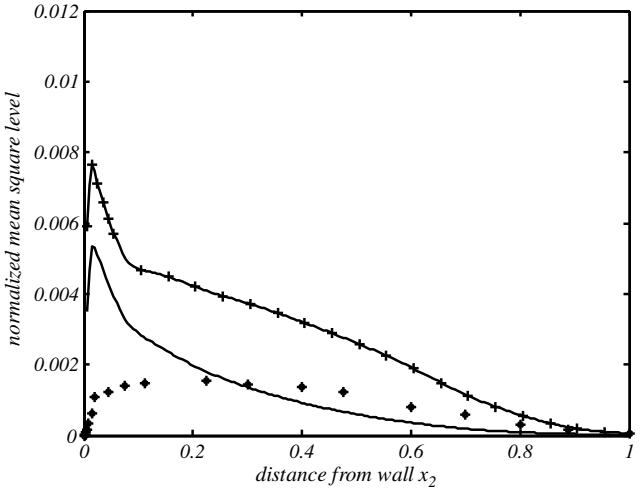

Fig. 3 The distribution of TKE and mean square of v_2 as a function of distance from the wall. The TKE distribution (plus sign), measurements of $\langle v_2^2\rangle$ by Klebanoff [10] (asterisks), and evaluation of $\langle v_2^2\rangle$ by the model (solid line).

assuming high-frequency fluctuations, which were not part of the measurement. To simulate the effect of frequency filtering on the inversion method, the energy spectrum of the turbulence was multiplied by $\exp(-3.3\lambda L)$, and the energy spectrum (shown in Fig. 4) was used for the inversion of the measured TKE. The corrected inversion is shown in Fig. 5. and the agreement between the measured and estimated values of the turbulent stress normal to the wall is remarkable, with only a small error close to $x_2 = 0.05$. While this result is not conclusive, it provides a consistent explanation as to why the inversion of the TKE shown in Fig. 3 is inaccurate.

VI. Numerical Calculations

A. Reynolds-Averaged Navier–Stokes Calculations for a NACA 0012 Airfoil

The method described previously relies on RANS calculations to provide the mean velocity and turbulence characteristics near an airfoil trailing edge. To validate the method, 2-D RANS calculations were performed on several NACA 0012 airfoil configurations studied by Brooks and Hodgson [8] and Brooks et al. [9]. Table 1 summarizes the test configurations and operating conditions that were analyzed.

The 2-D RANS calculations were performed using Y237, a computational fluid dynamics (CFD) code that has been developed at Pratt and Whitney over a number of years and has been used to solve a variety of steady and unsteady turbomachinery problems (e.g., Ni [13] and Prasad and Feng [14]). A description of Y237 can be found in those references.

Figure 6 shows the computational domain and the grid topology that was used for all RANS calculations in the present study. The airfoil leading edge was located at $x_1/c = 0$. The domain extended 10 chords upstream from the leading edge, 10 chords downstream from the trailing edge, and 10 chords above and below the airfoil axis. The domain was divided into five sectors consisting of 4 H grids and 1 C grid. The C grid was used to cluster points in the airfoil vicinity and provide good resolution of the trailing-edge boundary layer. For all the RANS cases, there were at least 35 grid points inside the trailing-edge boundary layer, including eight points in the viscous sublayer, with the first grid point located within $y^+ = 2$ from the airfoil surface. Uniform total pressure (10^5 N/m^2), total temperature (288 K), and axial velocity were imposed at the upstream boundary of the domain. The upstream boundary conditions for the k-ω turbulence model were chosen to simulate the freestream turbulence intensity values reported by Brooks and Hodgson [8] and Brooks et al. [9], which are shown in Table 1. The upper and lower boundaries were modeled as frictionless impermeable walls.

Figure 7 compares the RANS-calculated boundary-layer displacement thickness to the corresponding measurements reported in Brooks and Hodgson [8] and Brooks et al. [9]. The displacement thickness has been normalized by the airfoil chord and is plotted versus chord Reynolds number. The RANS calculations were done for a fully turbulent boundary layer growing from the leading to the trailing edge of the airfoil. The test data in [8] was acquired with a 2-cm-wide 40-grit trip located at $x_1/c = 15\%$, while the data in [9] was acquired with both a naturally transitioned boundary layer (i.e, untripped), and with a 60-grit trip extending from $x_1/c = 0$ to $x_1/c = 20\%$ (i.e., heavily tripped). The RANS calculations are reported at $x_1/c = 99.6\%$, which is consistent with the measurements in [8]. However, the measurements in [9] are reported at 1.3 mm downstream from the airfoil trailing edge, independent of the airfoil chord.

As expected, the RANS calculations fall between the heavily tripped and untripped measurements. Note that a power-law relationship, shown in Fig. 7, provides an excellent fit to the RANS calculations. The exponent of the curve fit (0.22) is similar to that reported for a flat plate turbulent boundary layer (0.20) over this Reynolds number range (e.g., Schlichting [15]). However, the coefficient (0.16) is larger than that for a flat plate (0.046), probably due to the effect of airfoil surface curvature and the resultant pressure gradient.

Figure 8 shows the mean velocity profiles at $x_1/c = 99\%$ for each CFD case. This chordwise location corresponds to the location used in subsequent noise predictions. The velocity profiles are plotted

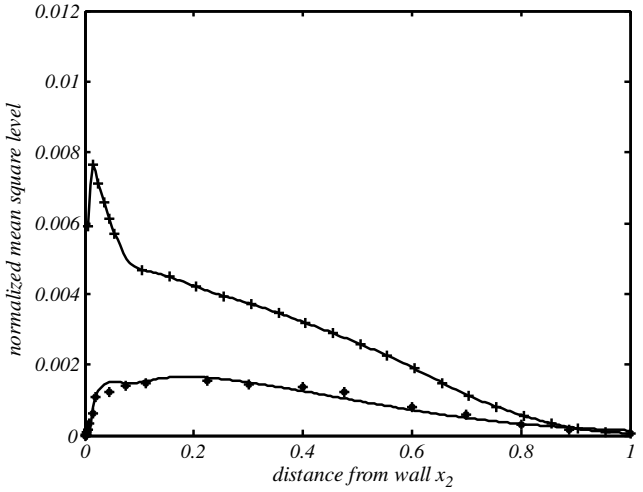

Fig. 5 The distribution of TKE and mean square of v_2 as a function of distance from the wall. The TKE distribution (plus sign), measurements of $\langle v_2^2 \rangle$ by Klebanoff [10] (asterisks), and evaluation of $\langle v_2^2 \rangle$ by the model with the modified spectrum (solid line).

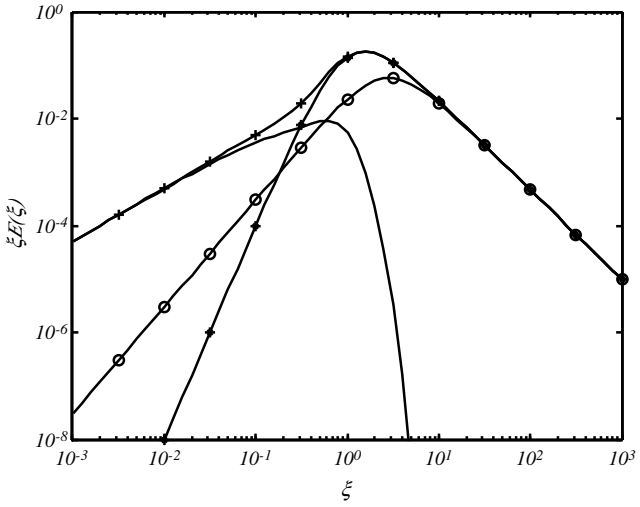

Fig. 4 The energy spectra used in the inversion technique (same legend as Fig. 2). The line shows the filtered spectrum used to obtain results in Fig. 5.

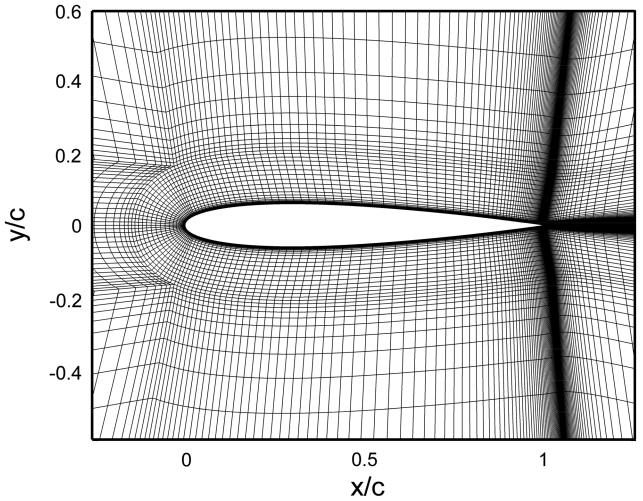

Fig. 6 Computational domain for RANS calculation of a NACA 0012 airfoil.

Table 1 NACA 0012 test configurations and operating conditions used for 2-D RANS calculations

CFD case	Airfoil chord, cm	Angle of attack, deg	Freestream velocity, m/s	Freestream turbulence, %	Chord Reynolds No. $\times 10^{-6}$	References
A	60.96	0	61.8	0.4	2.6	Brooks and Hodgson [8]
B	30.48	0	71.3	0.05	1.50	Brooks et al. [9]
C	30.48	0	55.5	0.05	1.16	Brooks et al. [9]
D	30.48	0	39.6	0.05	0.83	Brooks et al. [9]
E	30.48	0	31.7	0.05	0.67	Brooks et al. [9]
F	22.86	0	71.3	0.05	1.12	Brooks et al. [9]
G	15.24	0	71.3	0.05	0.75	Brooks et al. [9]
H	10.16	0	71.3	0.05	0.50	Brooks et al. [9]

versus the distance from the airfoil surface, normalized by the local boundary-layer displacement thickness. The velocity has been normalized by the axial velocity imposed at the upstream boundary of the domain. Presented in this manner, the mean velocity profiles are very similar for each case.

Figure 9 shows the calculated TKE and turbulent scale profiles at $x_1/c = 99\%$. The TKE has been normalized by the square of the upstream velocity, and the turbulent scale has been normalized by the local displacement thickness. Results show that the Reynolds number has a large effect on the peak normalized TKE, which varies from approximately 0.0055 to 0.0075. For $x_2/\delta^* \leq 1.5$, Reynolds number has little effect on the normalized turbulent scale, but has a large effect for $x_2/\delta^* > 1.5$.

B. Airfoil Self-Noise

The method described previously has been verified by considering the measurements of Brooks and Hodgson [8], who give both the surface pressure spectra and the radiated noise from an airfoil at zero angle of attack in an undisturbed stream. The blade section used was a NACA 0012 airfoil with a 0.6096 m chord in a flow with a speed of 69.5 m/s. The radiated noise was shown to be the result of the blade boundary layer interacting with the trailing edge and so we expect that the far-field noise spectrum should be predicted by Eq. (37).

To predict the flow, RANS calculations were carried out for the conditions corresponding to the experiment as described in the previous section. These provided the mean flow velocity profiles, the TKE profile, and the length-scale profile specified by Eq. (45).

The TKE profile at the trailing-edge location (99% chord) was inverted using the procedure described in Sec. IV and used in the numerical integration of Eq. (37) to estimate the radiated noise spectrum. Since Brooks and Hodgson's [8] measurements were in one-third octave bands, the narrow band spectra were corrected using the filter bandwidth to give the equivalent levels. The airfoil was at zero angle of attack. The noise was assumed to be generated by two identical boundary layers on either side of the blade and their contributions to the far-field noise was summed incoherently.

Figure 10 shows the comparison between the measured and the predicted noise spectrum for Brooks and Hodgson's [8] airfoil with good agreement between the measured and predicted spectra. The close agreement between the measurements and predictions prompted the evaluation of additional airfoil self-noise measurements by Brooks et al. [9] for NACA 0012 airfoils with chord ranging from 0.075 to 0.3028 m and flow speeds of 31.7 to 71.3 m/s. For these cases, there were some concerns about the tripping of the boundary layer close to the leading edge of the airfoil. In the measurements by Brooks et al. [9], various different boundary-layer trips were used, and in the RANS calculations, natural transition of the boundary layer was assumed. The tripping of the boundary layer has a significant effect on the boundary-layer thickness at the blade trailing edge and also on the radiated noise, so comparisons were made to the experimental measurements with different trip configurations. In general, it was found that the RANS calculations agreed with the lightly tripped cases given by the Brooks et al. [9] prediction code, which is consistent with the results given in Fig. 7.

The Brooks et al. [9] lightly tripped case uses a boundary-layer thickness that is 60% of the fully tripped boundary-layer thickness, whereas Fig. 7 indicates that the RANS calculations are 75% of the fully tripped boundary-layer thickness. Good agreement was found in each case at higher flow speeds (see Fig. 11), but at the lower flow speeds (Fig. 12), the predictions tend to overestimate the low frequencies and underestimate the higher frequencies by ~2 dB, but this could be accounted for by the RANS modeling of the boundary-layer trip.

Brooks and Hodgson [8] also measured the surface pressure beneath the boundary layer at a location 0.0254 m upstream of the trailing edge. Using the preceding and evaluating Eq. (39), predictions were also made of the surface pressure spectrum. However, it was found that the numerical integration of the double integral

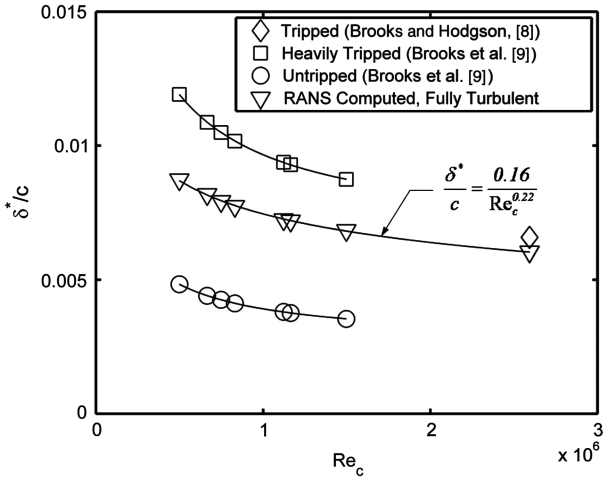

Fig. 7 Comparison of RANS-calculated trailing-edge displacement thickness to measurements reported by Brooks and Hodgson [8] and Brooks et al. [9].

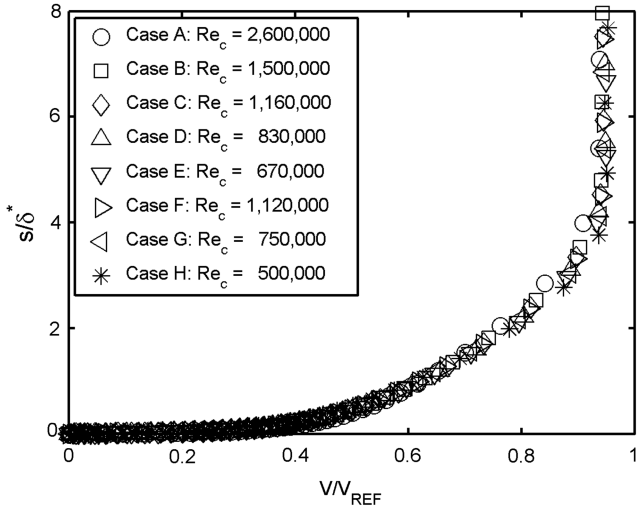

Fig. 8 Calculated mean velocity profiles at $x_1/c = 99\%$. The vertical axis is the distance from the wall normalized by the boundary-layer displacement thickness.

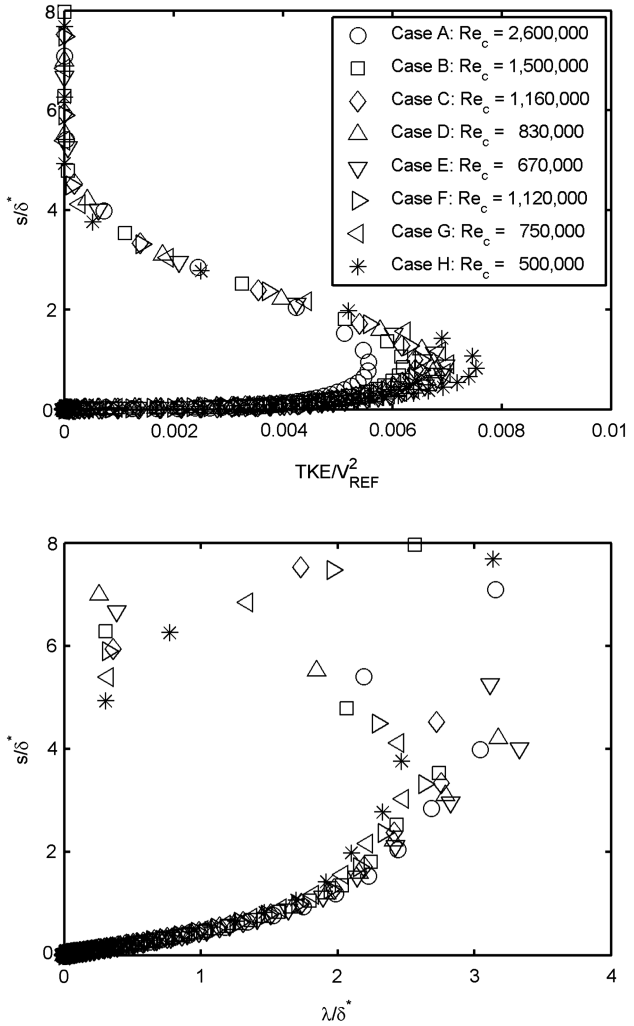

Fig. 9 Calculated turbulence characteristics at $x_1/c = 99\%$. The upper curve shows the TKE and the lower curve shows the turbulent scale on the horizontal axis. The vertical axis is the distance from the wall normalized by boundary-layer displacement thickness.

in Eq. (36) was time consuming and prone to error. An accurate approximation to the integral over k_3 was obtained by assuming that the integrand was dominated by the term λ_o^{-4} and assuming all the other terms are constant. An approximate form for Eq. (36) is then

$$S_{PP}(\omega) \approx \frac{(\rho_o U_\infty^2)^2 \delta_o}{U_\infty} \int_0^R \frac{\pi \omega A(y_o)}{2U_o^2} |P_e(y_o, \omega/U_o)|^2 E(\omega L/U_o)\, \mathrm{d}y_o \tag{48}$$

which can be computed quickly using numerical integration.

Figure 13 shows the predicted and measured spectra of Brooks and Hodgson's [8] surface pressure measurements. In this case, the levels at midfrequencies are well estimated but the levels at low and high frequencies are substantially underestimated. The theoretical spectrum given by Eq. (36) or Eq. (48) does not include the

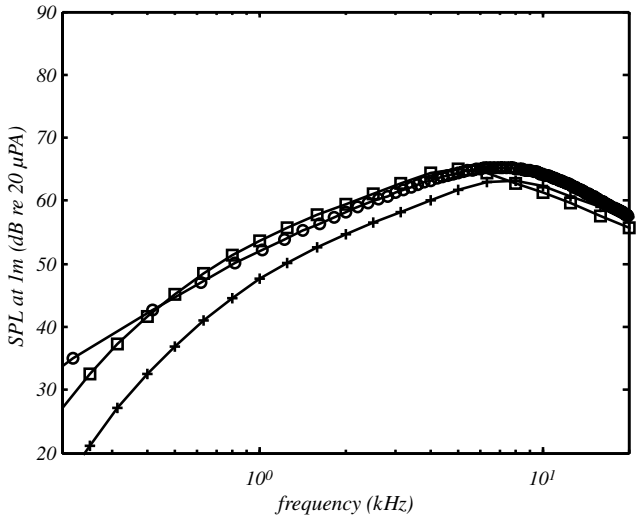

Fig. 11 Prediction of the SPL spectrum of trailing-edge noise from a NACA 0012 airfoil. Vertical axis shows SPL at 90 deg to the airfoil chord. The prediction is based on the inversion of a RANS k-ω model (circles) and from the empirical prediction method of Brooks et al. [9] (untripped: plus signs, lightly tripped: boxes). Airfoil chord is 0.1 m, and the flow speed is 71.3 m/s.

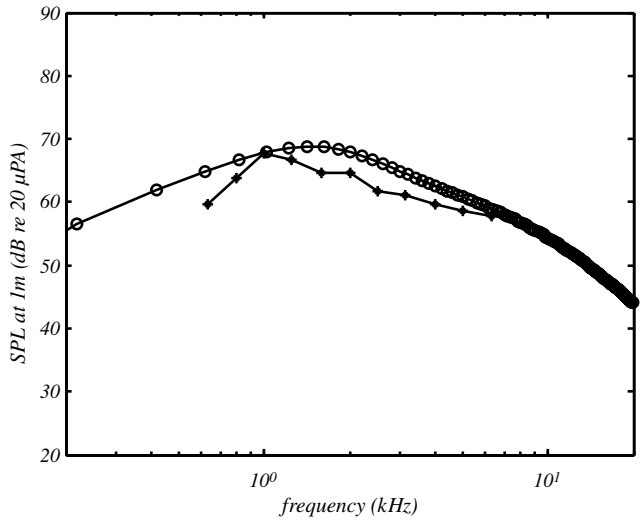

Fig. 10 Prediction (circles) and measurement (asterisks) of the sound pressure level (SPL) spectrum of trailing-edge noise from a NACA 0012 airfoil. Vertical axis shows SPL at 90 deg to the airfoil chord. The prediction is based on the inversion of a RANS k-ω model, and the measurements are by Brooks and Hodgson [8]. Airfoil chord is 0.6096 m, and the flow speed is 69.5 m/s.

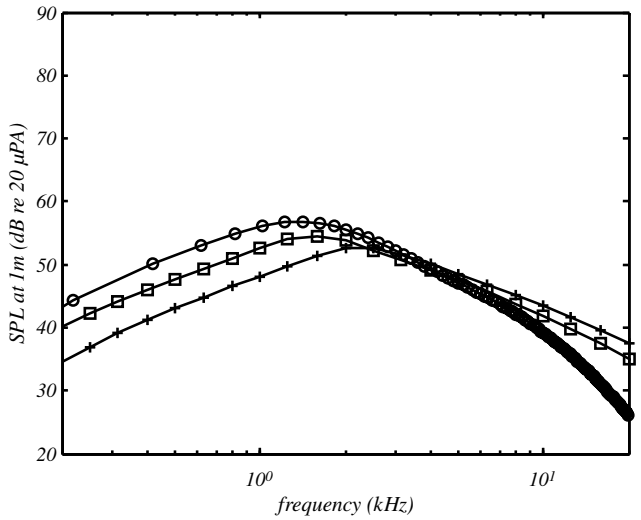

Fig. 12 Prediction of the SPL spectrum of trailing-edge noise from a NACA 0012 airfoil. Vertical axis shows SPL at 90 deg to the airfoil chord. The prediction is based on the inversion of a RANS k-ω model (circles) and from the empirical prediction method of Brooks et al. [9] (untripped: plus signs, lightly tripped: boxes). Airfoil chord is 0.3028 m, and the flow speed is 39.6 m/s.

scattering by the trailing edge, which will enhance the measured surface pressure levels close to the trailing edge. Howe [2] estimates that this effect will occur within one characteristic eddy length of the trailing edge, but it is an acoustic effect and so will be most important at low frequencies where the acoustic wavelength is largest. Consequently, the underestimate of the levels at low frequencies may be the result of the edge scattering. However, Brooks and Hodgson [8] showed that their data collapsed based on boundary-layer variables independently of the distance from the edge, and so the explanation of this discrepancy at low frequencies is not entirely clear. At frequencies below 1 kHz, facility noise is visible in the data. Above 2 kHz, where the rotor self-noise is significant, the facility noise drops to levels far below the fan self- noise.

C. Computation of Approach Power Fan Noise in the Fan Rig

In this section, we apply the trailing-edge noise model described previously to a 22 in. fan in the rig. Both aerodynamic performance and far-field noise measurements were made (Hughes et al. [16] and Woodward et al. [17]) in the NASA John H. Glenn Research Center at Lewis Field 9×15 low-speed anechoic wind tunnel. A unique feature of these measurements was the ability to isolate the rotor-alone noise from the rotor fan exit guide vane interaction noise. The rotor-alone noise was obtained using a rotor-alone nacelle configuration and the results presented in this section will be compared with the data taken from the rotor-alone configuration.

In what follows, results from a RANS simulation of the fan blade at the approach power were used. The mean flow quantities in the vicinity of the trailing edge along with the TKE and length scales were inputs into the self-noise formulation presented in this paper. Predictions of the sound power were then compared against noise data taken in the test.

Since the self-noise model is locally 2-D, the mean flow profiles and turbulence quantities are input at various radial strips, which go from the hub to the tip of the fan blade. Figure 14 shows the CFD profiles on both the suction and pressure sides of the fan blade at midspan. The trailing-edge region velocity profiles, the TKE profiles, and the turbulent length-scale profiles on the suction and pressure sides of the fan blade are shown in Figs. 14a–14c, respectively. The TKE is nondimensionalized by the freestream kinetic energy, the velocity profile is nondimensionalized by the freestream velocity, and the turbulent length scale is nondimensionalized by the boundary-layer thickness. The suction side has large TKE and shear due to the high velocities. The turbulent length scale is slightly smaller on the suction side. Note that the nondimensional velocity approaches unity at the edge of the boundary layer and the TKE goes

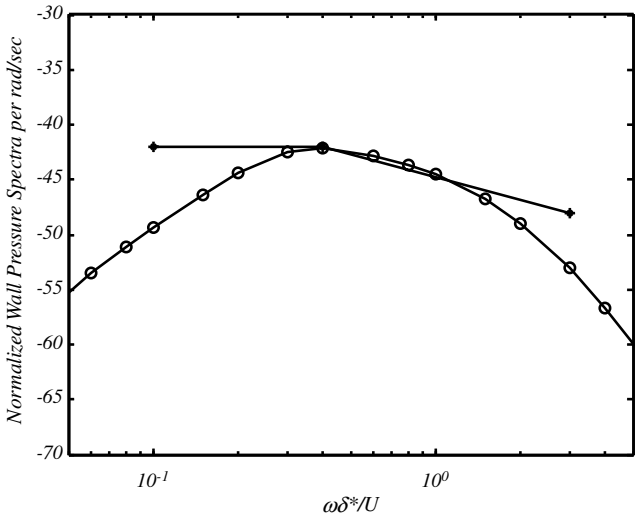

Fig. 13 Comparison between the predictions based on RANS calculations (circles) and the measured spectra (asterisks) by Brooks and Hodgson [8] of the surface pressure at the trailing edge of a NACA 0012 airfoil. Vertical axis shows the normalized power spectral density of surface pressure fluctuations in decibels.

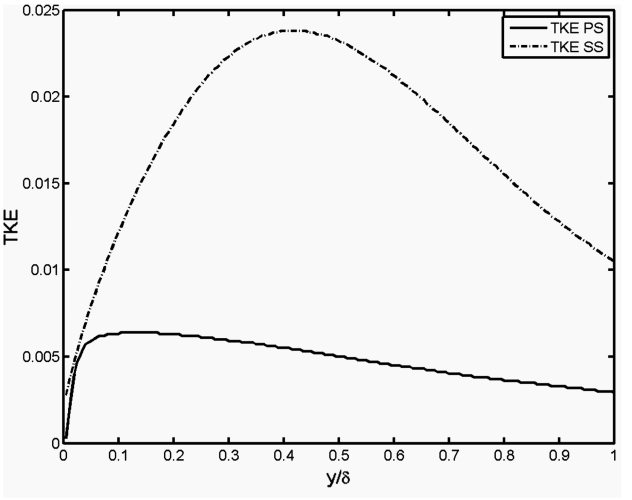

a)

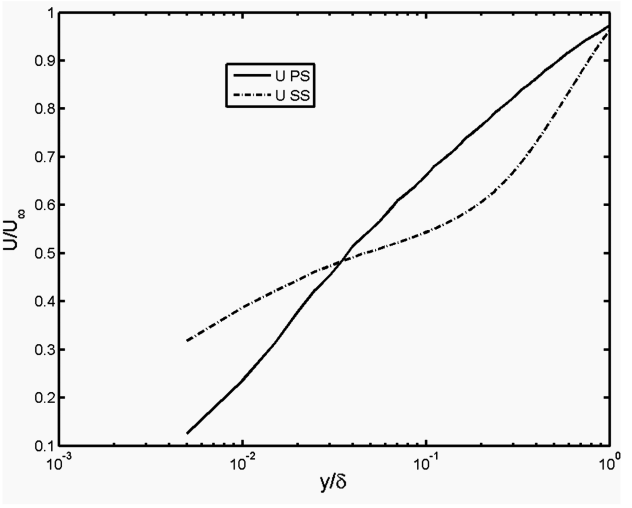

b)

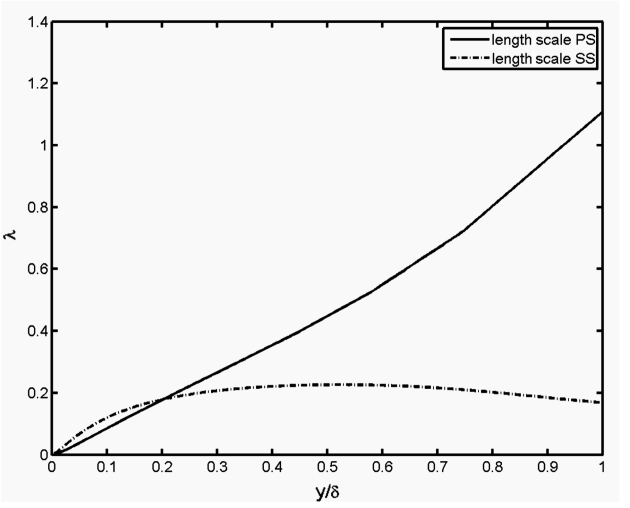

c)

Fig. 14 CFD profiles: a) the distribution of TKE versus distance away from the wall, b) the mean velocity versus distance from the wall, and c) the turbulent length-scale distribution versus distance from the wall. (PS denotes pressure side, SS denotes suction side, and U denotes velocity).

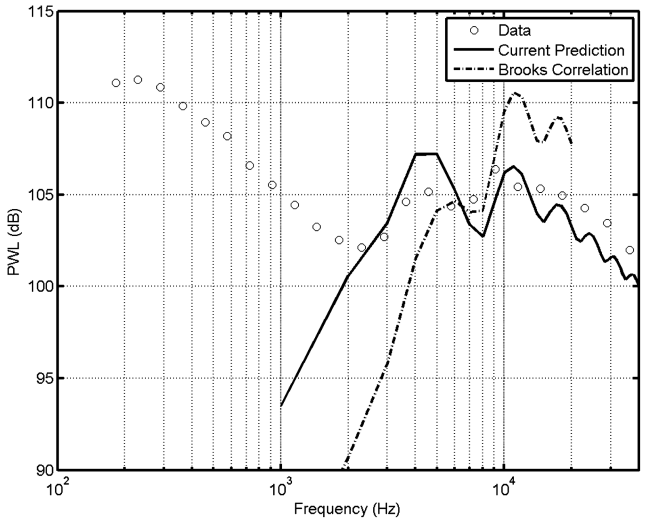

Fig. 15 The downstream sound power radiated from the fan blades versus frequency. The symbols correspond to the measured data: the solid line is the prediction based on the current model, and the dotted–dashed line is the prediction using the Brooks et al. [9] self-noise database.

to zero. These boundary-layer quantities are the inputs for the trailing-edge noise prediction, shown in Fig. 15.

Figure 15 shows the sound power predictions from the broadband fan noise prediction system self-noise model, which is based on the database presented by Brooks et al. [9], the self nose method based on RANS as presented here and the measured far-field noise data. The noise model based on RANS input falls within 1–2 dB of the measured data over the range of frequencies (4–20 kHz) where fan rotor self-noise is dominant. This is significantly better than the prediction based on the Brooks database predictions that overpredict the data over a wide frequency range by about 3–5 dB. The primary differences between the data and the RANS model are the oscillations that occur in the prediction. These oscillations are a result of interference effects due to blade to blade interference effects (Glegg [18]).

VII. Conclusions

The preceding results show how spatial distributions of TKE in a shear flow can be used to estimate spectral levels and two-point statistics of the flow. The procedure requires the solution to the linearized vorticity equation in a shear flow to be matched to TKE distributions, which can be obtained either from measurements, or alternatively from RANS calculations of the flow. Given the mean flow and TKE distribution from RANS calculations, the choice of spectrum and the length-scale model, there are no other inputs or adjustable constants in this procedure. The process is therefore applicable to a wide variety of problems, which can be considered as 2-D. Extensions to flows, which evolve in the direction of the flow have not been considered at this time but will be the subject of future work.

This study has shown the following.

1) The turbulent velocity fluctuations in a boundary layer can be directly related to a distribution of vortex sheet strength as a function of distance from the wall.

2. The TKE profile and surface pressure spectra can also be defined in terms of the vortex sheet strength.

3. Inverting a known TKE profile obtained from measurements or RANS calculations to obtain the vortex sheet strength provides the necessary information to estimate the surface pressure spectrum and the noise radiated by the interaction of the boundary layer with a sharp trailing edge.

4. The TKE profiles measured in a wind tunnel have been used to estimate the turbulent stress distribution and wall pressure spectra with some success if a correction is applied for the high-frequency response of the instrumentation.

5. The TKE profiles estimated from RANS calculations on an airfoil have been used to estimate radiated trailing-edge noise levels with good agreement for a number of different airfoils with a range of flow speeds and different chord lengths.

6. The measured and predicted far-field sound spectra of trailing-edge noise from a series of NACA 0012 airfoils with different chords were found to show the same dependence on flow speed and close agreement in absolute level and spectral shape.

7. The approach has been used to predict the self-noise from a small-scale fan rig with an accuracy of 1–2 dB.

Appendix

Writing Eq. (3) in transformed space and using Eq. (6d) to eliminate v_1, we can relate the vorticity to two components of the velocity in the form:

$$\hat{\omega}_1 = \frac{\partial \hat{v}_3}{\partial x_2} + ik_3\hat{v}_2 \tag{A1a}$$

$$\hat{\omega}_2 = \frac{i\lambda^2}{k_1}\hat{v}_3 - \frac{k_3}{k_1}\frac{\partial \hat{v}_2}{\partial x_2} \tag{A1b}$$

$$\hat{\omega}_3 = -ik_1\hat{v}_2 - \frac{\partial}{\partial x_2}\left(-\frac{k_3}{k_1}\hat{v}_3 + \frac{1}{ik_1}\frac{\partial \hat{v}_2}{\partial x_2}\right) \tag{A1c}$$

where $\lambda^2 = k_1^2 + k_3^2$. Using Eq. (A1), Eqs. (6a) and (6b) can then be expressed in terms of a pair of differential equations for the velocity components $\hat{v}_2$ and $\hat{v}_3$,

$$\hat{v}_2' = \frac{-ik_1U'}{\Lambda}\hat{v}_2 - \frac{\lambda^2}{ik_3}\hat{v}_3; \qquad \hat{v}_3' = -ik_3\hat{v}_2 + \frac{ik_1U'}{\Lambda}\hat{v}_3 \tag{A2}$$

where the primes denote differentiation with respect to the direction normal to the wall. If we set $u = \hat{v}_2$ and introduce $\frac{\omega}{k_1} = -U_0$, then using Eqs. (A2) and (6d), we obtain

$$\hat{v}_1 = -\frac{ik_1}{\lambda^2}\left(u' + \frac{k_3^2U'u}{k_1^2(U-U_o)}\right); \qquad \hat{v}_2 = u;$$
$$\hat{v}_3 = -\frac{ik_3}{\lambda^2}\left(u' - \frac{U'u}{(U-U_o)}\right) \tag{A3}$$

We can use the third of Eq. (7) and the second of Eq. (A2) to form a differential equation for u, which is given by Eq. (8).

Acknowledgments

Stewart Glegg would like to thank Pratt and Whitney for their support during the course of this project. The authors would like to thank Jinzhang Feng for his assistance and guidance on the Reynolds-averaged Navier–Stokes calculations.

References

[1] Amiet, R. K., "Noise Due to Turbulent Flow past a Trailing Edge," *Journal of Sound and Vibration*, Vol. 47, No. 3, 1976, pp. 387–393. doi:10.1016/0022-460X(76)90948-2

[2] Howe, M. S., *Acoustics of Fluid Structure Interactions*, Cambridge Univ. Press, Cambridge, England, U.K., 1998.

[3] Townsend, A. A., *The Structure of Turbulent Shear Flow*, Cambridge Univ. Press, Cambridge, England, U.K., 1978.

[4] Lee, Y-T., Blake, W. K., and Farabee, T. M., "Modeling of Wall Pressure Fluctuations Based on Time Mean Flow Field," *Journal of Fluids Engineering*, Vol. 127, No. 2, 2005, pp. 233–240. doi:10.1115/1.1881698

[5] Lutz, T., Herrig, A., Wurz, W., Kamruzzaman, M., and Kramer, E., "Design and Wind-Tunnel Verification of Low-Noise Airfoils for Wind Turbines," *AIAA Journal*, Vol. 45, No. 4, 2007, pp. 770–785. doi:10.2514/1.27658

[6] Spitz, N., "Prediction of Trailing Edge Noise from Two-Point Velocity Correlations," M.S. Thesis, Virginia Polytechnic Inst. and State Univ.,

Blacksburg, VA, 2005.
[7] Moser, R. D., Kim, J., and Mansour, N. N., "Direct Numerical Simulation of Turbulent Channel Flow up to $Re_\tau = 590$," *Physics of Fluids*, Vol. 11, No. 4, 1998, pp. 943–945. doi:10.1063/1.869966
[8] Brooks, T. F., and Hodgson, T. H., "Trailing Edge Noise Prediction from Measured Surface Pressures," *Journal of Sound and Vibration*, Vol. 78, No. 1, 1981, pp. 69–117. doi:10.1016/S0022-460X(81)80158-7
[9] Brooks, T. F., Pope, D. S., and Macolini, M. A., "Airfoil Self Noise and Prediction," NASA Reference Publ. 1218, 1989.
[10] Klebanoff, P. S., "Characteristics of Turbulence in a Boundary Layer with Zero Pressure Gradient," NACA Rept. 1247, 1955.
[11] Atassi, O. V., "Propagation and Stability of Vorticity-Entropy Waves in a Non-Uniform Flow," *Journal of Fluid Mechanics*, Vol. 575, March 2007, pp. 149–176. doi:10.1017/S0022112006004137
[12] Pope, S. B., *Turbulent Flows*, Cambridge Univ. Press, Cambridge, England, U.K., 2000.
[13] Ni, R., "A Multiple-Grid Scheme for Solving the Euler Equations," *AIAA Journal*, Vol. 20, No. 11, 1982, pp. 1565–1571. doi:10.2514/3.51220
[14] Prasad, D., and Feng, J., "Propagation and Decay of Shock Waves in Turbofan Engine Inlets," *Journal of Turbomachinery*, Vol. 127, No. 1, Jan. 2005, pp. 118–127. doi:10.1115/1.1811102
[15] Schlichting, H., *Boundary-Layer Theory*, 7th ed., McGraw–Hill, New York, 1979.
[16] Hughes, C. E., Jeracki, R. J., and Miller, C. J., "Fan Noise Source Diagnostic Test-Rotor-Alone Nacelle Aerodynamic Performance Results," AIAA Paper 2002-2426, June 2002.
[17] Woodward, R. P., Huges, C. E., Jeracki, R. J., and Miller, C. J., "Fan Noise Source Diagnostic Test Far-Field Acoustic Results," AIAA Paper 2002-2427, June 2002.
[18] Glegg, S. A. L., "Airfoil Self Noise Generated in a Cascade," *AIAA Journal*, Vol. 36, No. 9, 1998, pp. 1575–1582. doi:10.2514/2.583

D. Gaitonde
Associate Editor